Valence charge fluctuations in $YBa_2Cu_3O_{7-\delta}$ from core-level spectroscopies

A. Balzarotti, M. De Crescenzi, N. Motta, F. Patella, and A. Sgarlata
Dipartimento di Fisica, Università degli Studi di Roma II, via Orazio Raimondo, I-00173 Roma, Italy
(Received 27 June 1988)

From x-ray photoemission and Auger measurements of the Cu $2p$ and O $1s$ core levels of $YBa_2Cu_3O_{7-\delta}$ as a function of the oxygen concentration δ, the average copper charge is determined. Evidence is found of dynamic charge fluctuations on the oxygen sublattice giving rise to a greater concentration of trivalent copper at the Cu(1) sites with respect to that determined by the analysis of neutron-diffraction data. One the basis of our experimental results, we introduce a molecular cluster description for the Cu states. The lowest final-states configurations of Cu^{2+} and Cu^{3+} are $\underline{c}3d^{10}\underline{L}$ and $\underline{c}3d^{10}\underline{L}^2$, respectively, where $\underline{c}$ and $\underline{L}$ denote core holes on copper and oxygen atoms. Oxygen holes have high mobility and a Hubbard correlation energy less than 2 eV, a signature of their delocalization. The effect of temperature on the spectra is minor. Surface degradation modifies the relative intensity of the structures, particularly those of the O spectrum.

I. INTRODUCTION

The ceramic oxides $YBa_2Cu_3O_{7-\delta}$—the so-called 1:2:3 compounds—which exhibit superconductivity above 90 K,[1] can be described as mixed-valence systems where Cu acquires 2+ and 3+ valence in the superconducting state. The concentration of Cu in the highest oxidation state is strongly correlated to the oxygen content, i.e., to the vacancy concentration δ. The final Cu^{3+} content after a thermal cycle depends upon the temperature of annealing and on the cooling rate.[2] Annealing in O_2 atmosphere up to 400 °C involves a continuous uptake of oxygen into the lattice until saturation through the exothermic reaction $YBa_2Cu_3{}^{2+}O_{6.5} \rightarrow YBa_2Cu_2{}^{2+}Cu_1{}^{3+}O_{7-\delta}$ and a corresponding saturation of the $[Cu^{3+}]/[Cu^{2+}]$ ratio to 0.5.[3] Subsequent heating up to 950 °C removes oxygen from the system and reduces Cu^{3+} back to Cu^{2+}. In addition, the Cu^{1+} species is observed.[4] Concomitantly to the change in the oxygen stoichiometry from 6.5 to 7, the structure undergoes a tetragonal-to-orthorhombic structural transition[5-7] and the critical temperature T_c increases from 0 to ≈ 90 K.[8] It is believed that trivalent copper could play a crucial role in the mechanism of the superconductivity, particularly the one based on bipolarons' condensation. An important issue in this context is the site occupied by Cu^{3+} in the unit cell. A preferential occupancy of the Cu(1) sites on the Cu-O one-dimensional chains (Fig. 1) rather than on the Cu(2) sites has been reported.[4,9]

The determination of the Cu^{3+} species by the use of high-energy spectroscopies [x-ray photoemission spectroscopy (XPS), x-ray-absorption spectroscopy (XAS), and extended x-ray absorption fine-structure spectroscopy (EXAFS)] has provided results confirming,[4,10,11] disproving[12-16] or doubting[17] the existence of trivalent ions even in samples with δ close to zero. The reason for this discrepancy is, in our opinion, twofold. First, the average fraction of Cu in the trivalent state is 33% of the total Cu ions for $\delta = 0$ and is a fraction of this for $\delta \neq 0$. This is a rather large concentration but the transition involving Cu^{3+} is expected to occur 1.5–2 eV above the transition involving Cu^{2+} (Ref. 13) in XPS and $\cong 2$ eV in XAS.[10] Therefore, a small concentration of O vacancies (i.e., $\delta \approx 0$) and a high-energy resolution are needed to resolve these two components. The second reason is of a more fundamental nature. The existence of the formal 3+ valence does not imply a well-defined Cu^{3+} species on a given lattice site, but the electron deficiency (hole) can be distributed between the copper and the oxygen ions to form charged $(Cu^{3+}\text{-}O^{2-})^+$ (a hole on the Cu^{2+} ion) and $(Cu^{2+}\text{-}O^-)^+$ (a hole on the O^{2-} ion) complexes. The mixed valence of the oxygen is favored by the presence of excess oxygen and by the overlapping of the Cu $3d$ and O $2p$ states forming the valence band. In a molecular orbital description, the ground-state configuration of the Cu^{3+} is $\alpha|3d^8\rangle + \beta|3d^9\underline{L}\rangle + \gamma|3d^{10}\underline{L}^2\rangle$, where $\underline{L}$ and $\underline{L}^2$ denote one and two holes on the ligand, respectively. Photoemission data on CuO (Ref. 18) and configuration-interaction calculations on a CuO_6 cluster (Ref. 19) indicate that the divalent $3d^9\underline{L}$ multiplet has the lowest energy, whereas the d^8 state is about 10 eV above the Fermi energy. Thus, the Cu^{3+} ground state is mainly divalent

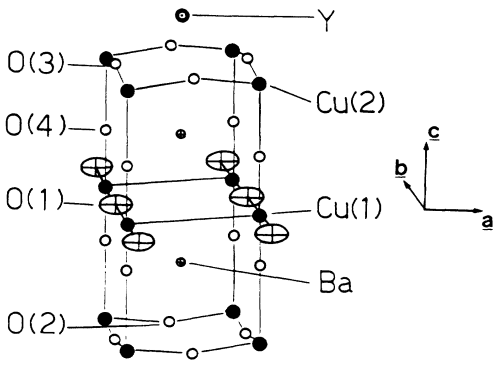

FIG. 1. Orthorhombic structure $YBa_2Cu_3O_{7-\delta}$ showing the thermal ellipsoids in the Cu(1)-O(1) a-b plane.

and nearly degenerate with the $|3d^9\rangle + |3d^{10}\underline{L}\rangle$ Cu^{2+} ground state, and the mixing with the trivalent d^8 configuration is small ($\alpha < \beta, \gamma$). Since the ordering of the final-state levels probed by x-ray photoemission is reversed compared to that of absorption,[20] the XPS well-screened threshold states will have predominantly $\underline{c}d^{10}\underline{L}$ and $\underline{c}d^{10}\underline{L}^2$ character, while XAS states will be mainly $\underline{c}d^{10}$ ($\underline{c}$ denotes a core hole). It follows that XPS spectra contain pieces of important information about the nonionic part of the Cu-O band, i.e., about the hole transfer from the Cu to the O valence states. On the other hand, XAS final states reflect mainly the divalent components of the Cu^{2+} and Cu^{3+} clusters which dominate the ground-state configuration.

In this paper, we report high-resolution XPS and Auger measurements taken on well-characterized single-phase $YBa_2Cu_3O_{7-\delta}$ samples ($\delta < 0.2$) above the Cu $L_{2,3}$ and O K edges. The spectra indicate clearly the presence of trivalent copper and support a mechanism of *dynamic* valence fluctuation on the oxygen sublattice with a screened Coulomb repulsion among delocalized holes in the O band. The importance of a dynamically fluctuating charge on the superconductivity has been already underlined.[21] Modification of the intensities, spectral shapes and energy position of the structures at low temperature ($T = 80$ K) in the superconducting phase are minor except for the Cu $L_{2,3}VV$ Auger spectrum.

II. EXPERIMENT

A. Sample preparation and characterization

The samples of $YBa_2Cu_3O_{7-\delta}$ were prepared by mixing fine powders of 99.99% pure Y_2O_3, $BaCO_3$, and CuO in stoichiometric ratio Y:Ba:Cu=1:2:3 and, subsequently, pressing them into pellets. They were then sintered at 950 °C for 10 h in flowing pure O_2 atmosphere and then slowly furnace cooled down ($\cong$2 °C/min) to prevent loss of oxygen. The four-point Van der Pauw method gave a sharp drop of the resistance at 92 ± 2 K. X-ray analysis showed the presence of a single phase with orthorhombic structure. Thermal gravimetric analysis (TGA) yielded an oxygen vacancy concentration $\delta \simeq 0.2$. A second set of samples was prepared with the citrate pyrolisis technique described elsewhere.[22] The average grain size of the sintered samples ($\cong 1$ μm) was smaller than that of samples grown by the ceramic method, which resulted in a smoother surface with uniform distribution of grains, as shown by electron micrography. Resistivity as a function of temperature was measured and yielded a transition temperature of 93 ± 2 K (Fig. 2). Magnetic susceptibility measurements as a function of temperature in small fields ($B < 6$ G) and zero-field cooling configuration indicate an exclusion of the magnetic flux larger than 93% at 77 K and $\cong$100% at 4.2 K for fully oxygenated samples. The lattice structure was determined by neutron-powder-diffraction measurements at 300 K. Diffraction data were subjected to the Rietveld refinement[23] to obtain the structural parameters (Fig. 3). The oxygen positions were based on the ideal perovskite structure and refined along with the oxygen site occupancies. The results (Table I) indicated an orthorhombic structure (*Pmmm* space group) with oxygen stoichiometry in the range 6.8–6.9 ($\delta \cong 0.15$). Oxygen vacancies are located at the O(1) site on a line parallel to the b axis. The fact that the Cu(1)–O(4) bond (1.839 Å) is much more stretched than the Cu(1)–O(1) bond (1.934 Å) and the large thermal factor B_{11} suggest a coupling to the electronic motion through the in-plane breathing mode of the oxygen.[24]

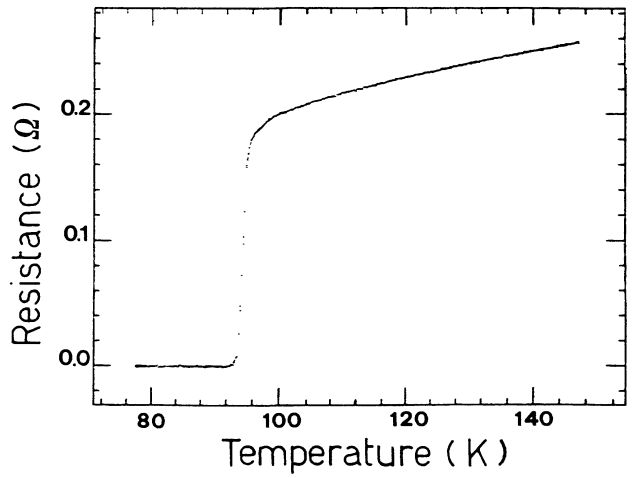

FIG. 2. Resistance as a function of temperature for $YBa_2Cu_3O_{6.85}$.

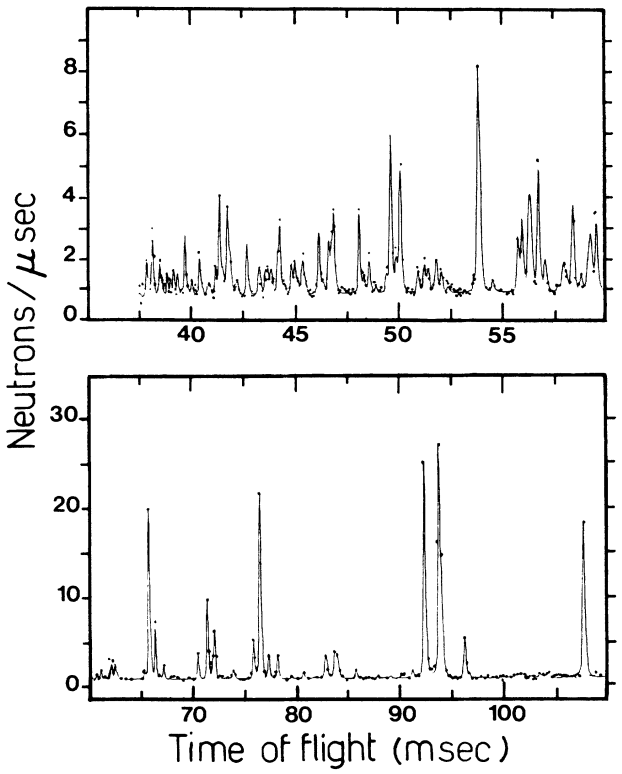

FIG. 3. Rietveld refinement profiles for the orthorhombic $YBa_2Cu_3O_{6.85}$. The points represent the raw neutron powder diffraction data and the solid line is the calculated profile. The d spacing ranges from 0.75 to 2.2 Å.

TABLE I. Structural parameters for $YBa_2Cu_3O_{7-\delta}$ determined from the Rietveld refinement of neutron-powder-diffraction data. Anisotropic thermal factors are defined as $\exp(B_{11}^2h^2+B_{22}^2k^2+B_{33}^2l^2)$. $a=3.8196$ Å, $b=3.8789$ Å, $c=11.6719$ Å, $V=172.969(4)$ Å^3.

Atom	x/a	y/b	z/c	B_{iso} (Å^2)	Site occ.	Mult.
Y	0.5	0.5	0.5	0.9(7)	1.000	1
Ba	0.5	0.5	0.1853	1.3(7)	1.000	2
Cu(1)	0.0	0.0	0.0000	0.8(8)	1.000	1
Cu(2)	0.0	0.0	0.3553	1.4(4)	1.000	2
O(1)	0.0	0.5	0.0000	a	0.84(7)	1
O(2)	0.5	0.0	0.3791	1.2(3)	1.000	2
O(3)	0.0	0.5	0.3785	1.1(3)	1.000	2
O(4)	0.0	0.0	0.1516	1.2(5)	1.000	2

[a]For O(1), the anisotropic temperature factors are $B_{11}=2.6(3)$ Å^2, $B_{22}=1.0(9)$ Å^2, $B_{33}=0.8(7)$ Å^2.

B. X-ray analysis

XPS and Auger measurements were done in ultrahigh vacuum (UHV) (base pressure $<1\times10^{-10}$ Torr) using a twin anode (Al and Mg) x-ray source and a VG Clam 100 electron hemispherical analyzer. The overall energy resolution was about 1.1 eV. During the chamber bakeout process at 120 °C, the samples were kept at room temperature by flowing water through the sample holder to avoid any oxygen loss due to heating. The partial pressures of the residual gases in the chamber were monitored by a VG Arga quadrupole gas analyzer. Before each set of measurements we scraped the sample *in situ* to expose fresh superconducting grains of correct stoichiometry. The surface conditions were often checked by performing wide XPS scans. The main contaminant observed was carbon, probably segregated at the grain boundaries, a residue of barium carbonate used in the synthesis of the compound. Unscraped or air-exposed samples have an oxygen concentration different from that of bulk, due, probably, to surface contamination. We found that spectra taken after different scrapes were quite reproducible but not identical. Since no loss of oxygen was detected during the scraping process, we believe that these differences are intrinsic to the different individual grains exposed after the mechanical scraping rather than due to sample inhomogeneities. To minimize the experimental uncertainty, we have recorded several spectra for each run in order to reach statistical significance. The measurements were made at 300 and 80 K and at a few intermediate temperatures. The temperature was measured with a Chromel-Alumel thermocouple fixed close to the sample surface.

In some cases, after several runs and thermal cycles in UHV, a progressive intensity reduction of some structures was noted, particularly those associated with oxygen. These aging effects are indicative of changes in the surface chemical composition and/or of surface degradation under x-ray irradiation. In such cases, a new scrape usually reverted back the surface to the previous conditions. Copper reduction[25] and surface oxidation stages[26] in copper oxides are well documented in the literature.

III. RESULTS

We focus first on the Cu $2p$ core-level spectra where the largest effects have been observed. In Fig. 4, we report the spectrum of $YBa_2Cu_3O_{6.85}$ measured at room temperature after background subtraction. The spectrum exhibits the spin-orbit components Cu $2p_{3/2}$ and Cu $2p_{1/2}$ at binding energies ≈933 and ≈953 eV, respectively, with their satellites at ≈9-eV higher binding energy. From the comparison with the CuO spectrum,[4] these transitions are the final states of the Cu^{2+} ion in the oxygen environment. A remarkable feature to note is the extra peak at ≈2.5 eV from the main $2p_{3/2}$ peak. The existence of this structure has been previously inferred from line-shape analyses[4,11] but not clearly observed as in the present experiment. It is strongly correlated to the oxygen deficiency δ and tends to be quickly washed out for $\delta>0.3$. We believe that it is responsible for the already noted and unexplained[4] broadening of the divalent copper line with respect to the trivalent one. We assign this transition to Cu^{3+}. This point will be discussed later.

In Figs. 5 and 6, the Cu $2p_{3/2}$ portion of the spectrum

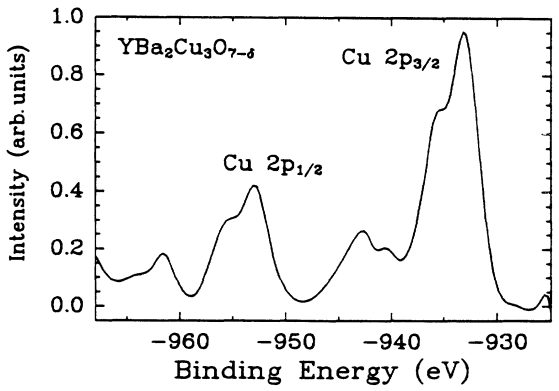

FIG. 4. Cu $2p$ XPS spectrum of $YBa_2Cu_3O_{6.85}$ pellets measured at $T=300$ K after background subtraction. Notice the peak on the high-binding energy side of the spin-orbit doublet.

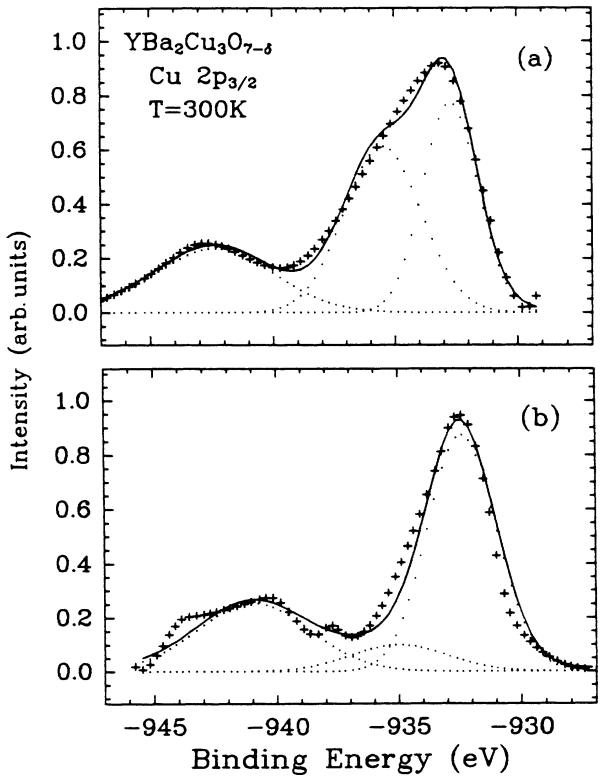

FIG. 5. Cu $2p_{3/2}$ spectra of $YBa_2Cu_3O_{7-\delta}$ for (a) stoichiometric ($\delta=0.15$) and (b) oxygen-deprived surfaces, measured at $T=300$ K with background removed. Fit (solid lines) to the experiment (+) using three Gaussian components (dotted lines).

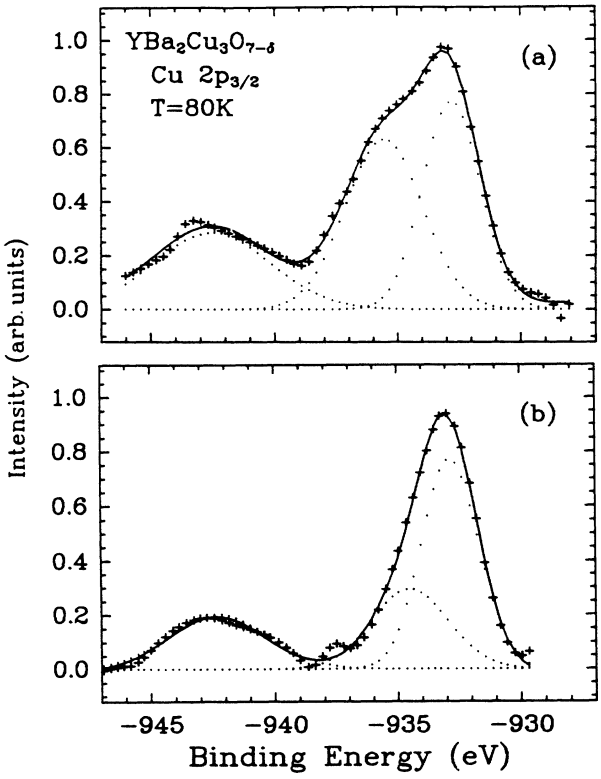

FIG. 6. Cu $2p_{3/2}$ spectra of $YBa_2Cu_3O_{7-\delta}$ for (a) stoichiometric ($\delta=0.15$) and (b) oxygen-deprived surfaces, measured at $T=80$ K with background removed. Fit (solid lines) to the experiment (+) using three Gaussian components (dotted lines).

has been fitted with three Gaussians to estimate the relative weights I_A and I_C of the Cu^{2+} component and that I_B of the Cu^{3+} component. From them we can determine the Cu^{3+}/Cu^{2+} fraction $R=I_B/(I_A+I_C)$ and the average number $n_{Cu^{3+}}$ of Cu^{3+} ions. They are listed in Table II for two different temperatures and vacancy concentrations δ. We notice a slight increase of their average values (although within the rms deviation) in the superconducting phase. From the comparison of Figs. 5 and 6, we are not able to recognize significant changes between the semiconducting ($T=300$ K) and superconducting ($T=80$ K) phases, while a significant attenuation of the Cu^{3+} intensity occurs in both cases after loss of oxygen [panel (b) in both Fig. 5 and 6]. A similar reduction with increasing δ has been recently observed in samples having $\delta > 0.24$.[11]

The O 1*s* spectra around 530 eV binding energy are shown in Fig. 7. They consist of two main structures *A* and *B* at 528.9 and ≈ 532 eV, respectively, and a weak

TABLE II. Oxygen vacancy concentration δ, critical temperature T_c, binding energies of the peaks and corresponding area ratios from XPS spectra. $n_{Cu^{3+}}$ is the average Cu^{3+} concentration and T the temperature of the measurements. $R=I_A/I_B$ for oxygen.

δ	Edge	E_A (eV)	E_B (ev)	E_C (eV)	R	$n_{Cu^{3+}}$	T (K)
0.15	Cu $2p_{3/2}$	932.8 ± 0.1	935.6 ± 0.5	943.5 ± 0.9	0.52 ± 0.11	0.32 ± 0.06	300
					0.56 ± 0.10	0.40 ± 0.07	80
0.15	O 1*s*	528.8 ± 0.2	532.6 ± 0.2	534.0 ± 0.5	0.22 ± 0.15		300
0.20	Cu $2p_{3/2}$	932.8 ± 0.1	935.2 ± 0.4	942.5 ± 0.5	$0.43+0.10$	0.27 ± 0.06	300
					0.46 ± 0.13	0.31 ± 0.07	80
0.20	O 1*s*	528.5 ± 0.3	532.3 ± 0.6	534.2 ± 0.8	0.27 ± 0.12		300
					0.20 ± 0.13		80

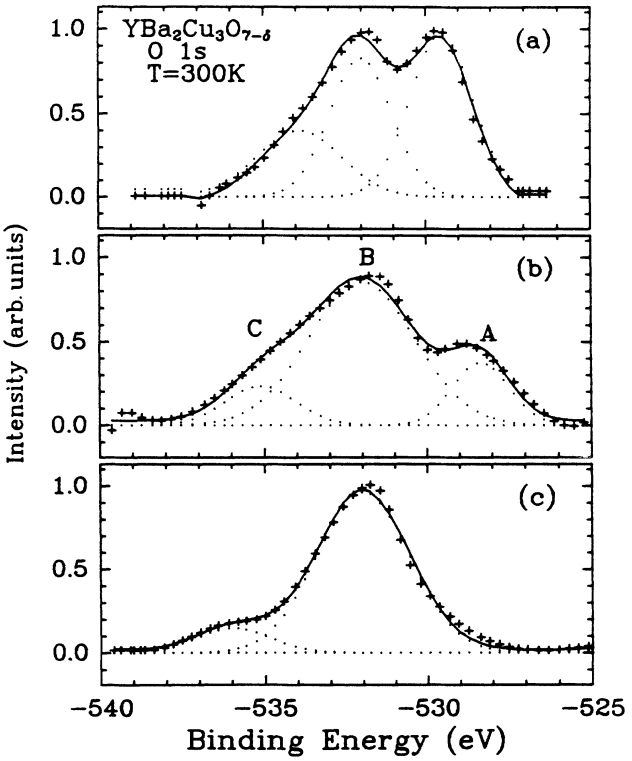

FIG. 7. O 1s XPS spectra of $YBa_2Cu_3O_{7-\delta}$ for different surface conditions. Panel (c) corresponds to the highest surface contamination. Fit (solid lines) to the experiment (+) using three Gaussians components (dotted lines). Notice the broadening of the structures giving from (a) to (c). Background has been removed.

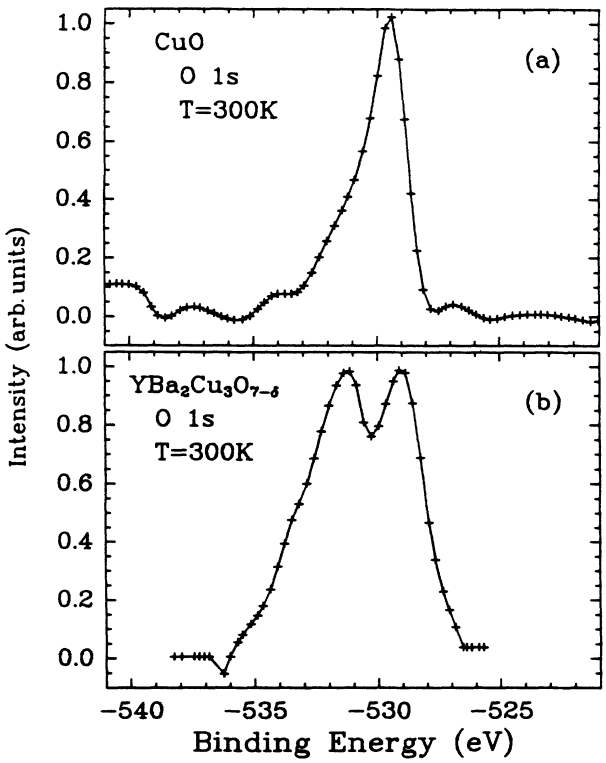

FIG. 8. Comparison between the O 1s spectra of CuO [panel (a)] and of $YBa_2Cu_3O_{7-\delta}$ after background subtraction.

structure around 535 eV. Here, the effect of surface contamination is particularly severe. Peak A, which is higher than B in freshly scraped surfaces, gradually reduces till it disappears in fully contaminated surfaces [Fig. 7(c)]. We consider the spectra with the lowest B/A ratio equal to 0.68 as representative of the uncontaminated surface. It is worth noticing from Fig. 8 that peak A corresponds to the main peak CuO, suggesting a common origin for both. For most surfaces exposed to air A and B intensities are inverted.

Since the exposed surfaces are intrinsically different because the distribution, size, and oxygen content of each grain differs after every each scrape, we have averaged over several scans (typical larger than 20) to reduce spreading. Table III contains the average peak positions and the relevant intensity ratio for the Cu $2p_{3/2}$ edges. Figure 9 displays the distribution of these data. It should be noted that the broad distribution of the A/B ratio around 0.22 ± 0.15 for the oxygen reflects the prevalent occurrence of surfaces for which the A peak is smaller than B. This situation is characteristic of chemisorbed O_2 —probably at the surface of the grains—which is removed after heating in vacuum at about 450 °C.[27]

In Figs. 10 and 11 we show the Cu $L_3M_{4,5}M_{4,5}$ and the O $KL_{2,3}L_{2,3}$ Auger spectra after background subtraction according to the Shirley[28] prescription. The copper spectrum displays an extra peak, besides the main component, at kinetic energies of about 915 eV which is larger at lower δ's and increases and shifts slightly to higher binding energies with decreasing temperature. It decreases strongly in oxygen-deprived samples, paralleling the behavior of the peak B of oxygen, and has been discussed in a separate paper.[29]

TABLE III. Measured and calculated (values in brackets) relative binding energies positions ΔE_{ij} and satellite-to-main peak intensity ratios for the Cu $2p_{3/2}$ core-level and electronic structure parameters (defined in the text).

Sample	ΔE_{AB} (eV)	ΔE_{AC} (eV)	I_C/I_A	T	T'	Δ	U_{hh} (eV)	Q	n_d
$YBa_2Cu_3O_{6.85}$	2.8 ± 0.6 (2.83)	10.7 ± 1.0 (10.2)	0.35 ± 0.2 (0.29)	2.8	0	0.0	2	8.5	9.5
$YBa_2Cu_3O_{6.80}$	2.4 ± 0.5 (2.32)	9.7 ± 0.6 (9.70)	0.32 ± 0.2 (0.28)	2.7	0	0.0	1.5	8.1	9.5

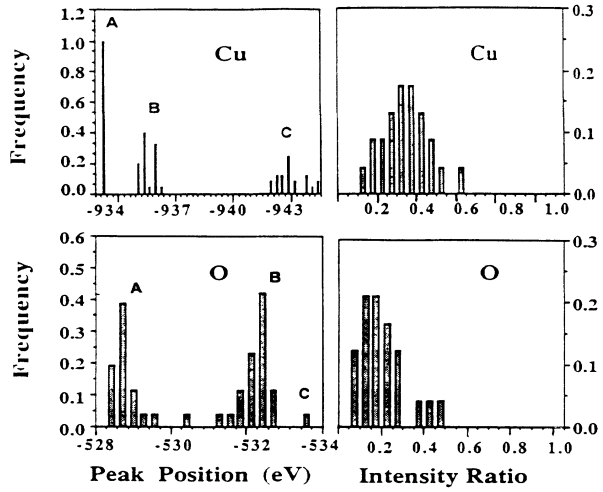

FIG. 9. Measured statistical distributions of the peaks' positions and intensity area ratios for Cu and for O, respectively.

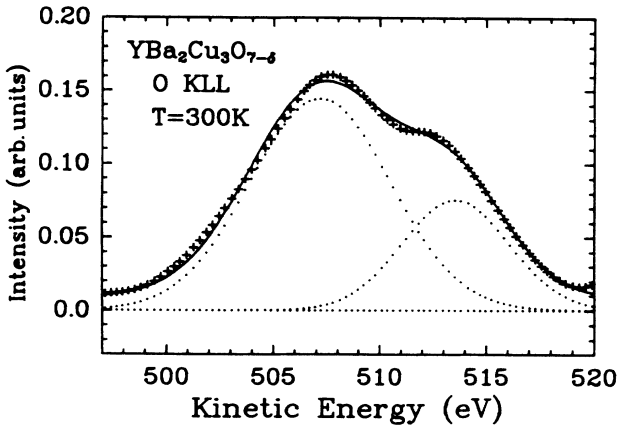

FIG. 11. O $KL_{2,3}L_{2,3}$ Auger spectrum of $YBa_2Cu_3O_{7-\delta}$ measured at $T=300$ K after background subtraction. Dotted lines are the component subspectra of the fit (solid line) to the experiment (+).

The oxygen Auger spectrum at 300 K, which is associated with the 1s level at 528.9 eV, consists of two broad structures located approximately at 507 and 514 eV and does not show a clear modification below T_c.

IV. DISCUSSION

A. Photoemission spectra

1. Cu 2p

Let us first discuss the core-level spectra of the Cu $2p_{3/2}$ at 932.8 eV. The neutron-diffraction data of Table I indicate that the O(1) site at (0,1/2,0) is partially vacant and possesses anomalously large and anisotropic thermal factors compared to the other oxygens. Moreover, the Cu(1)–O(4) bond distance (1.839 Å) is considerably shorter than the other Cu–O bond lengths lying between 1.93 and 1.96 Å. As already noted,[24] this suggests a preferential occupation of the Cu(1) site by Cu^{3+}. Applying the Brown and Wu[30] bond-strength analysis to the refined data, as done by David *et al.*,[24] we calculate an average valence of 2.0 for Cu(2) and of 2.28 and 2.56 for Cu(1) depending upon whether 2+ or 3+ valence is assumed. From charge neutrality considerations, the average charge of Cu(1) on the CuO_4 planar unit is $3-2\delta$, which implies a static mixture of 70% Cu^{3+} and 30% Cu^{2+} for the refined value $\delta=0.15(3)$. Thus the Cu^{2+}-Cu^{3+} valence mixing on the specific Cu(1) site gives a $[Cu^{3+}]/[Cu^{2+}]$ ratio $R=(1-2\delta)/[2(1+\delta)]=0.30$ or, equivalently, an average fraction of trivalent copper $n_{Cu^{3+}}=(1-2\delta)/3=0.23(2)$.

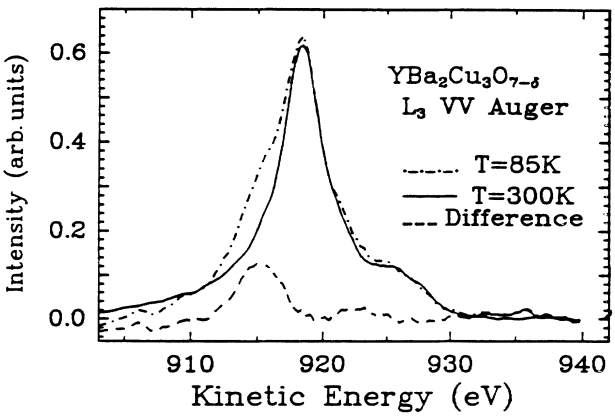

FIG. 10. Cu $L_3M_{4,5}M_{4,5}$ Auger spectra of $YBa_2Cu_3O_{7-\delta}$ measured at 300 and 85 K and their difference spectrum (dashed line). The background has been removed according to Ref. 28.

The above quantities can be directly compared with those derived from the Cu $2p_{3/2}$ spectra of Figs. 5 and 6. If we assume that the peak at 935.3 eV is due to the excitation of trivalent copper and the other peaks to that of divalent copper, for both sets of samples, we measure the R and $n_{Cu^{3+}}$ values reported in Table II. It appears that about 10% of trivalent Cu^{3+} ions, corresponding to an average number d of Cu^{3+} ions, are present in addition to the Cu^{3+} ions located in the chains, as shown by the neutron-diffraction analysis. In this case, the ionic binding energy per molecule will be lowered by a few eV.[31] Alternatively, the Cu-O_4 layer would contain O^- ions, where the oxygen holes are highly mobile, because of their hybridization with the Cu orbitals. In any case, the Cu^{3+} final-state wave function will contain, besides the ionic part, a sizable covalent part. This latter component is associated with a single-electron transfer from the metal Cu^{2+} ion to the O^- atoms giving a O^{2-} and a Cu^{3+} configuration. The average number of Cu^{3+} ions will be $n_{Cu^{3+}}=[(1-2\delta)+d]/3$ and the average $[Cu^{3+}]/[Cu^{2+}]$ ratio will be

$$R=\frac{(1-2\delta)+d}{2(1+\delta)-d}. \quad (1)$$

These quantities are plotted in Fig. 12 for $d=0$ (dashed lines) and $d=0.33$ (solid lines) as a function of the vacancy concentration δ and compared with the XPS data of Table II. The better agreement with experiment for

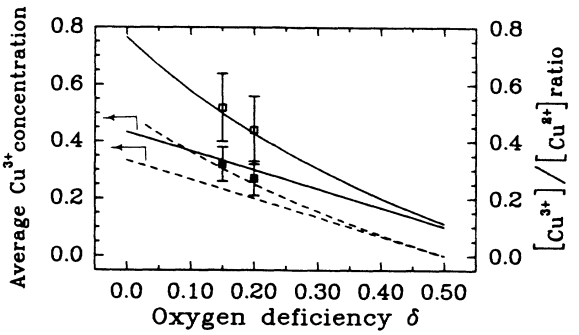

FIG. 12. Average $[Cu^{3+}]/[Cu^{2+}]$ ratio (right-hand scale) and average concentration of Cu_{3+} ions (left-hand scale) estimated from the Cu $2p$ spectra as a function of the oxygen vacancy concentration δ (squares). Dashed lines: calculated neglecting oxygen charge fluctuation ($d=0$); solid lines: calculated including oxygen charge fluctuation ($d=0.33$).

$d=0.33$ suggests the existence of an extra contribution due to the valence fluctuation on the oxygen atoms.

We adopt a small cluster to represent the central Cu atom surrounded by four oxygen ligands in the b-c plane. We describe the ground state of this cluster embedded in an effective medium in the extended configuration interaction scheme as a superposition of $3d^9$ and $3d^{10}\underline{L}$ states for Cu^{2+} and of $3d^8$, $3d^9\underline{L}$, and $3d^{10}\underline{L}^2$ states for Cu^{3+}, in agreement with the previous evidence of a large copper to oxygen hybridization. It is likely that the d^8 component is excluded from the ground state because of its 10-eV excitation energy relative to the Fermi level[18] and the weight of $3d^{10}\underline{L}^2$ is small because of the double excitation on the ligand. If we take into account the delocalization of the holes, the final $3d^9\underline{L}$ and $3d^{10}\underline{L}^2$ states are denoted by $|3d^9\underline{L}k\rangle$ and $|3d^{10}\underline{L}^2\rangle$, respectively, where k are delocalized (band) electrons. Thus the Cu^{3+} ground state has predominantly a divalent $|3d^9\underline{L}k\rangle$ configuration. The *final* eigenstates are determined from the diagonalization of the Hamiltonian matrix

$$\begin{vmatrix} -E & T & 0 \\ T & -E-Q+\Delta & T' \\ 0 & T' & -E-Q+U_{hh} \end{vmatrix}, \qquad (2)$$

where $\Delta=\langle d^{10}\underline{L}|H|d^{10}\underline{L}\rangle-\langle d^9|H|d^9\rangle$ is the charge-transfer energy, Q the core-hole d-electron Coulomb interaction, and $T=\langle d^9|H|d^{10}\underline{L}\rangle$ and $T'=\langle d^{10}\underline{L}|H|d^{10}\underline{L}^2\rangle$ are the mixing matrix elements in the final state.[32] The excited $|\underline{c}3d^9\underline{L}\rangle$ state decays into the well-screened shake-down state $|\underline{c}3d^{10}\underline{L}^2k\rangle$ whose energy depends on the Coulomb repulsion U_{hh} on the O $2p$ band. How much the latter configuration is close to the $\underline{c}3d^{10}\underline{L}$ configuration depends upon the degree of correlation between holes. Delocalized holes will be largely screened from each other and U_{hh} will be small.

The best fit of the Cu $2p_{3/2}$ XPS spectra of Figs. 5 and 6 provides the parameters listed in Table III. The final-state picture for Cu is characterized by the lack of hybridization between the Cu^{3+} and Cu^{2+} cluster states and a small ($U_{hh}=1.5-2$ eV) Hubbard repulsion between the O holes which is indicative of their delocalization. The other parameters listed in Table III, i.e., the transfer integral T, the satellite-to-main peak ratio and the d-electron occupation in the ground state n_d are close to those obtained from valence-band photoemission spectra[19] and validate the conclusions of a strong electronic correlation on the copper site and a large covalency of the copper-oxygen bond. In particular, n_d is equal to 9.5, which is consistent with a mixture of d^9 and d^{10} configurations in the ground state. We remark that the Cu^{2+} and Cu^{3+} states are not mixed in the final state since $T'=0$. This implies that previous estimates[19] for these parameters without including trivalent basis states, are basically correct. From the present results, there is not clear evidence of temperature dependence for these quantities, as reported by other studies,[33] in which the trivalent component has not been considered.

2. O 1s

On the basis of the above conclusions, the O $1s$ XPS spectrum of Fig. 7 is of particular interest. An average number of 0.3 trivalent copper atoms per formula unit means that ≈ 0.7 oxygen atoms (10% of the O atoms) should adopt O^{-1} valence, since there are 2.3 oxygens per 1 copper. If we believe that the peak B at ≈ 532 eV is associated with the O(1) and O(4) atoms and the peak A at 529 eV with four O(2) and O(3) atoms of the CuO_2 plane, we estimate a peak ratio $(3-\delta)/4=0.7$ for δ equal to 0.15–0.2. This value is close to the B/A ratio observed for the best surfaces. Thus, the results of the O $1s$ spectra indicate that peak A is associated with the $\underline{1s}2p^6 3d^{10}\underline{L}$ final-state configuration and the B peak with the $\underline{1s}2p^6 3d^{10}\underline{L}^2$ configuration, respectively. The oxygen core hole, corresponding to O^{2-} ($1s$), is locally well-screened by the intra-atomic $2p^6$ electrons in the final state, and the Cu-O states are described by the initial-state configuration of Cu^{2+} and Cu^{3+}, respectively. However, because of the surface reactivity which affects the peaks' intensities, the above assignment for the oxygen structures must be taken with caution.

B. Auger spectra

1. Cu $L_3M_{4,5}M_{4,5}$

The Cu $L_3M_{4,5}M_{4,5}$ spectrum, shown in Fig. 10, has been already discussed by us[29] using the Cini-Sawatzky model.[34] Here, we reconsider it in the context of the molecular cluster states to provide further insight. The relevant two-hole final basis states of Cu to consider are $3d^8\underline{L}$, and $3d^7$ for divalent copper and the $3d^8\underline{L}^2$ for trivalent copper. The $3d^7$ state is at an energy of $\approx 3U_{dd}-\Delta$, too far from the ground-state energy to concern us, where U_{dd} is the large (7–8 eV) correlation energy between $3d$ electrons.[35] The $3d^8\underline{L}$ state originates from the $\underline{2p}3d^{10}\underline{L}$ state and it is found at a binding energy of $932.8-918.0=14.8\pm0.4$ eV, which corresponds to the main peak ^1G of the Auger spectrum. The $3d^8\underline{L}^2$ state which does not hybridize with $3d^8\underline{L}$, is expected to be

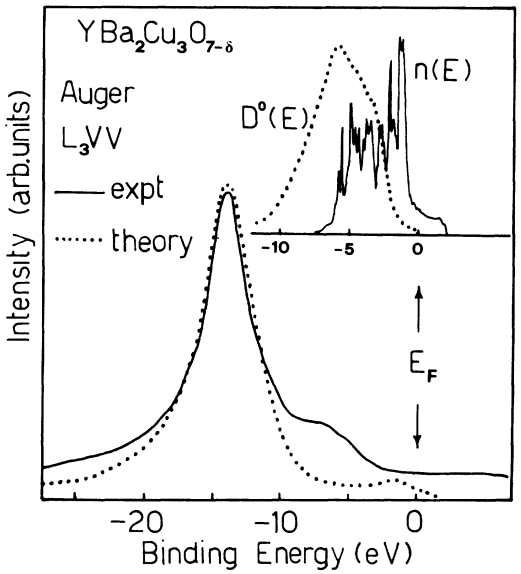

FIG. 13. Measured and calculated Auger $L_3M_{4,5}M_{4,5}$ profiles with $U_{dd}=7$ eV. The inset shows the theoretical total density of states (after Ref. 38) and its self-convolution $D^0(E)$. The zero of the binding energy scale is the Fermi energy.

(and it is found) above this state by almost the same energy which separates the $\underline{2p}3d^{10}\underline{L}$ and $\underline{2p}3d^{10}\underline{L}^2$ states, that is approximately the repulsive energy between the oxygen holes. The important thing to notice is the already-mentioned small value for the hole-hole repulsion in comparison to that estimated for localized holes (≈ 4.5 eV),[36] and the strong dependence of the $3d^8\underline{L}^2$ state on the surface conditions, similar to that of the B peak of the O $1s$ spectrum. We have observed[29] a temperature dependence for this peak that could be due to an enhanced correlation in the final two-hole states or to the effect of residual chemisorbed species.[27] In any case, the great sensitivity of this structure to the surface stoichiometry reflects the strong hybridization of the copper-oxygen bond.

In a previous analysis[29] of the Auger profile, using the Cu valence-band projected densities of states from Ref. 37, we estimated $U_{dd}\approx 2$ eV, much smaller than the correlation energy of the Cu metal (≈ 8 eV). Here we have recalculated this energy using the partial densities of states from Temmerman *et al.*[38] who used an improved Cu–O bond length. The results of this calculation, shown in Fig. 13, agree with the previous conclusions,[29] and provide an effective correlation energy $U_{dd}\approx 7$ eV closer to that of other estimates[19,35,36] with values of U_{dd} of 8.5 eV for Cu_2O and 9.6 eV for CuO.[18]

2. $OKL_{2,3}L_{2,3}$

The O $KL_{2,3}L_{2,3}$ spectrum of Fig. 11 clearly shows the doublet components forming the broad Auger spectrum. The largest peak at 507 eV is typical of a large number of bulk oxides[39] and corresponds to the quasi-atomic $^1D_2$ component of the final state (two-hole in the L shell) configuration $2s^22p^4$ of the chemisorbed O^{2-} ion. The structure at higher kinetic energy (≈ 514 eV) is more difficult to interpret. It is tempting to assign it to O^-, but other explanations are possible. In PtO_2 a similar high-energy peak is recognized as due to oxygen atoms adsorbed on the oxide layer[39] or to interatomic transitions. Since for this structure we have observed a clear dependence of surface conditions, we prefer to stick to the first explanation for this (intense) peak. From the binding energies of the O $1s$ peaks of Fig. 7 and from the oxygen valence band centroid (≈ 3.5 eV) (Ref. 38) we estimate a correlation hole-energy of ≈ 14 eV for the $^1D_2$ state and of 3–4 eV for the 514 eV peak. The former value suggests intra-atomic screening, similar to that of other transition-metal oxides,[40] while the latter indicates extra-atomic relaxation energy, comparable to the valence bandwidth. This value is closer to the effective Hubbard interaction energy calculated for localized oxygen holes[36] but still larger than that obtained from the analysis of the Cu $2p$ spectra.

V. CONCLUSIONS

We have used a combination of x-ray-photoemission and Auger core-level spectroscopies to investigate charge fluctuation on Cu and O sites. All spectra display features which are clear signatures of an oxidation state larger than the formal divalent state. The comparison with neutron-diffraction data and local charge neutrality analysis suggest a *dynamic* valence fluctuation on the oxygen sublattice—probably on the O(4) atoms in the Ba plane—due to the presence of the O^- species. Based on this evidence, we have developed a molecular description for the copper states. The lowest final-state configurations for Cu^{2+} and Cu^{3+} are $3d^{10}\underline{L}$ and $3d^{10}\underline{L}^2$, respectively, while the $3d^8$ configuration is excluded from the basis set. The lowest cluster states of Cu^{2+} and Cu^{3+} are not significantly hybridized in the final state. A number of parameters, which define the molecular states, are computed and found in good agreement with previous estimates. Hole wave functions are largely delocalized on the O $2p$ valence band and their correlation energy is less than 2 eV, much smaller than the that estimated for localized holes. Effects of surface degradation have been observed, particularly on the oxygen spectrum.

ACKNOWLEDGMENTS

The authors wish to acknowledge R. Messi, F. Celani, and M. Capizzi for the supply and characterization of the samples and C. Andreani, V. Merlo, and W. I. F. David for the neutron-diffraction measurements at the Isis neutron facility of the Rutheford Appleton Laboratories, England. This work has been supported by the Italian Centro Interuniversitario di Struttura della Materia-Gruppo Nazionale di Struttura della Materia.

[1]M. K. Wu, J. R. Ashburn, C. J. Torng, P. H. Hor, R. L. Meng, L. Gao, Z. J. Huang, Y. Q. Wang, and C. W. Chu, Phys. Rev. Lett. **58**, 908 (1987).
[2]H. Eickenbusch, W. Paulus, R. Schollhorn, and R. Schlogl, Mater. Res. Bull. **22**, 1505 (1987).
[3]P.Strobel, J. J. Capponi, C. Chaillout, M. Marezio, and J. L. Tholence, Nature (London) **327**, 306 (1987).
[4]P. Steiner, S. Hufner, V. Kinsinger, I. Sander, B. Siegwart, H. Schmitt, R. Schulz, S. Junk, G. Schwitzgebel, A. Gold, C. Politis, H. P. Muller, R. Hoppe, S. Kemmler-Sack, and C. Kunz, Z. Phys. B **69**, 449 (1988).
[5]I. V. Schuller, D. G. Hinks, M. A. Beno, D. W. Capone II, L. Soderholm, J. P. Locquet, T. Bruynseraede, C. U. Serge, and K. Zhang, Solid State Commun. **63**, 385 (1987).
[6]J. D. Jorgensen, M. A. Beno, D. G. Hinks, L. Soderholm, K. J. Volin, R. L. H. Herman, J. D. Grace, I. V. Schuller, C. U. Segre, K. Zhang, and M. S. Kleefisch, Phys. Rev. B **36**, 3608 (1987).
[7]G. Van Tenderloo, H. W. Zandbergen, and S. Amelinckx, Solid State Commun. **63**, 389 (1987).
[8]J. D. Jorgensen, B. W. Veal, W. K. Kwok, G. W. Crabtree, A. Umezawa, L. J. Nowicki, and A. P. Paulikas, Phys. Rev. B **36**, 5371 (1987).
[9]G. Xiao, M. Z. Cieplak, A. Gavrin, F. H. Streitz, A. Bakhshai, and C. L. Chien, Phys. Rev. Lett. **60**, 1446 (1988).
[10]A. Bianconi, A. Congiu-Castellano, M. De Santis, P. Rudolf, P. Lagarde, A. M. Flanck, and A. Marcelli, Solid State Commun. **63**, 1009 (1987).
[11]T. Gourieux, G. Krill, M. Maurer, M. F. Ravet, A. Menny, H. Tolentino, and A. Fontaine, Phys. Rev. B **37**, 7516 (1988).
[12]P. Steiner, V. Kinsinger, I. Sander, B. Siegwart, S. Hufner, C. Politis, R. Hoppe, and H. P. Muller, Z. Phys. B **67**, 497 (1987).
[13]A. Bianconi, A. Congiu-Castellano, M. De Santis, P. Delogu, A. Gargano, and R. Giorgi, Solid State Commun. **63**, 1135 (1987).
[14]D. Sarma and C. N. Rao, Solid State Commun. **65**, 47 (1988).
[15]N. Fukushima, H. Yoshino, H. Niu, M. Hayashi, H. Sasaki, Y. Yamada, and S. Murare, Jpn. J. Appl. Phys. **26**, L719 (1987).
[16]S. Horn, J. Cai, S. A. Shaheen, Y. Jeon, M. Croft, C. L. Chang, and M. L. den Boer, Phys. Rev. B **36**, 3895 (1987).
[17]The interpretation of the EXAFS results, reported so far, is quite controversial on the specific issue of the copper valence.
[18]M. R. Thuler, R. L. Benbow, and Z. Hurick, Phys. Rev. B **26**, 669 (1982).
[19]A. Fujimori, E. Takayama-Muromachi, Y. Uchida, and B. Okai, Phys. Rev. B **35**, 8814 (1987).
[20]G. van der Laan, J. Zaanen, G. A. Sawatzky, R. Karnatak, and J. M. Esteva, Phys. Rev. B **33**, 4253 (1986).
[21]R. A. de Groot, H. Gutfreund, and M. Weger, Solid State Commun. **63**, 451 (1987).
[22]F. Celani, R. Messi, S. Pace, and N. Sparvieri, Il Nuovo Saggiatore **4**, 7 (1988) (in Italian).
[23]The analysis was based on the Cambridge Crystallography Subroutine Library (CCSL), Rutheford Appleton Laboratory, England.
[24]W. I. F. David, W. T. A. Harrison, J. M. F. Gunn, O. Moze, A. K. Soper, P. Day, J. D. Jorgensen, D. G. Hinks, M. A. Beno, L. Soderholm, D. W. Capone II, J. K. Schuller, C. U. Segre, K. Zhang, and J. D. Grace, Nature (London) **327**, 310 (1987).
[25]T. H. Fleish and G. J. Mains, Appl. Surf. Sci. **10**, 51 (1982).
[26]K. Wandelt, Surf. Sci. Rep. **2**, 1 (1982).
[27]W. K. Ford, C. T. Chen, J. Anderson, J. Kwo, S. H. Liou, M. Hong, G. V. Rubenacker, and J. E. Drumheller, Phys. Rev. B **37**, 7924 (1988).
[28]D. A. Shirley, Phys. Rev. B **5**, 4709 (1972).
[29]A. Balzarotti, M. De Crescenzi, C. Giovannella, R. Messi, N. Motta, F. Patella, and A. Sgarlata, Phys. Rev. B **36**, 8285 (1987).
[30]I. D. Brown and K. K. Wu, Acta Crystallogr. B **32**, 1957 (1976).
[31]F. J. Adrian, Phys. Rev. B **37**, 2326 (1988).
[32]G. van der Laan, C. Westra, C. Haas, and G. A. Sawatzky, Phys. Rev. B **23**, 4369 (1981).
[33]S. Kohiki, T. Hamada, and T. Wada, Phys. Rev. B **36**, 2290 (1987).
[34]M. Cini, Solid State Commun. **24**, 681 (1977); G. A. Sawatzky, Phys. Rev. Lett. **39**, 504 (1977).
[35]J. C. Fuggle, P. J. W. Weijs, R. Schoorl, G. A. Sawatzky, J. Fink, N. Nucker, P. J. Durham, and W. M. Temmerman, Phys. Rev. B **37**, 123 (1988).
[36]H. Chen, J. Callaway, and P. K. Misra, Phys. Rev. B **38**, 195 (1988).
[37]L. F. Mattheiss and D. R. Hamann, Solid State Commun. **63**, 395 (1987).
[38]W. Temmerman, Z. Szotek, P. J. Durham, G. M. Stocks, and P. A. Sterne, J. Phys. F **17**, L319 (1987).
[39]P. Légaré, G. Maire, B. Carrière, and J. P. Deville, Surf. Sci. **68**, 348 (1977).
[40]P. Humbert and J. P. Deville, J. Electron. Spectros. Rel. Phenom. **36**, 131 (1985).

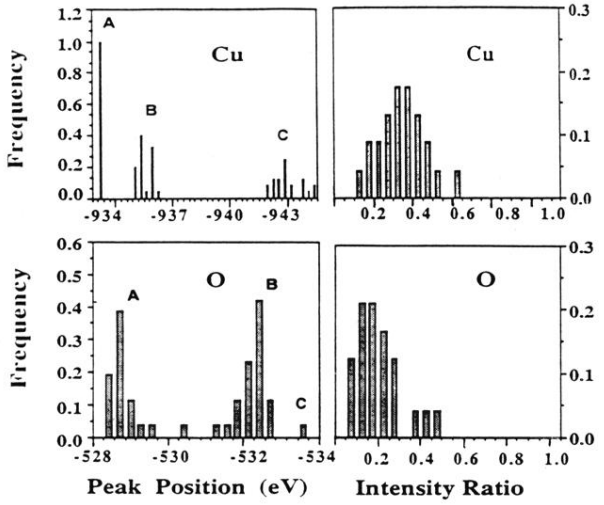

FIG. 9. Measured statistical distributions of the peaks' positions and intensity area ratios for Cu and for O, respectively.